

THE POLARISATION OF SECOND HARMONIC CORONAL TYPE III BURSTS

A. J. WILLES and D. B. MELROSE

Department of Theoretical Physics and Research Centre for Theoretical Astrophysics, School of Physics, University of Sydney, Australia

(Received 9 September, 1996; in final form 15 November, 1996)

Abstract. The process of second harmonic plasma emission is considered, where two simplifying approximations made in previous treatments are relaxed. The revised theory can account for strong polarisation observed in some harmonic coronal type III bursts, and predicts that a correlation between these bursts and the fastest electron beam speeds associated with type III emission should be apparent. These high observed degrees of polarisation could not be explained in the earlier theory. In most cases, polarisation in the sense of the magnetoionic *o*-mode is predicted. The predicted degree of polarisation is shown to be strongly dependent on the form of the Langmuir wave number spectrum, and in particular on the magnitude of the wave number offset between beam-driven and backscattered Langmuir waves.

1. Introduction

The purpose of this paper is to extend the theory for the polarisation of second harmonic plasma emission in coronal type III bursts to where two commonly used simplifying approximations are no longer valid. These are the head-on approximation, where it is assumed that the wave numbers of the coalescing Langmuir waves far exceed that of the product transverse electromagnetic waves, and the weak-field approximation, where the coronal magnetic field is assumed to be weak, so that the electron cyclotron frequency Ω_e is far smaller than the plasma frequency ($\Omega_e \ll \omega_p$). This work is motivated by the need to account for a number of observed harmonic type III bursts which are more strongly polarised than previous theory can plausibly explain.

Significant circular polarisation observed in coronal type III bursts is related to the strength of the coronal magnetic field. With the introduction of a magnetic field, the electromagnetic transverse mode separates into two modes with opposite senses of rotation of the electric field vector (e.g., Melrose, 1986, p. 171). For the magneto-ionic *x*-mode, the electric field vector rotates in the same sense as the gyration of an electron in a magnetic field. The magnetoionic *o*-mode electric field vector rotates in the opposite sense. The degree of circular polarisation r is a measure of the fraction of the emission that is circularly polarised. For $r = 1$ the emission is fully *o*-mode radiation; for $r = -1$ the emission is fully *x*-mode radiation.

A comprehensive study of the polarisation of 714 fundamental-harmonic pairs in the frequency range 24–220 MHz (Dulk and Suzuki, 1980) made the following

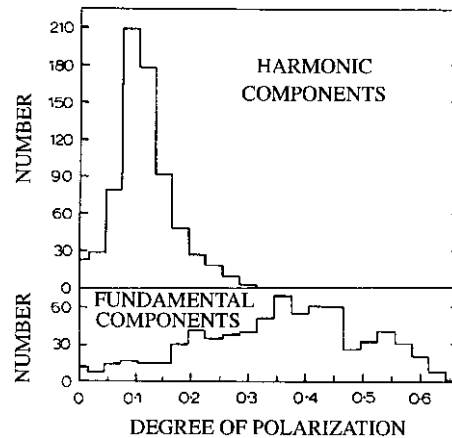


Figure 1. Observed degree of circular polarisation r for 714 fundamental-harmonic pairs (Dulk and Suzuki, 1980).

conclusions, many of which confirmed those of earlier studies: (i) The sense of polarisation of the fundamental and harmonic components is usually the same, and corresponds to o -mode radiation. (ii) The degree of circular polarisation is generally higher for the fundamental component; i.e., $r_F > r_H$. (iii) For the harmonic bursts, r strongly peaks about 0.1 and is observed in the range $0 \leq r \lesssim 0.3$. Figure 1 is a histogram of the observed degree of polarisation for both the fundamental and harmonic components. (iv) r_H is typically independent of frequency in the observed range of frequencies.

More recent measurements of the degree of circular polarisation for ‘structureless’ type III bursts (where the fundamental component is suppressed and only the harmonic component is observed) in the frequency range 164–435 MHz have been made (Mercier, 1990). In contrast to the observations of Dulk and Suzuki (1980), the degree of circular polarisation generally increases with frequency, from $r_H \approx 0.05$ at 164 MHz to $r_H \approx 0.15$ –0.20 at 435 MHz, which from the theory for second harmonic emission suggests that Ω_e/ω_p decreases with distance from the Sun (Mercier, 1990).

The theory for the polarisation of type III bursts assumes that nonlinear wave–wave interactions are responsible for the fundamental and harmonic emission. General formulas for the polarisation of fundamental and harmonic type III bursts were first derived by Melrose and Sy (1972) for an arbitrary distribution of Langmuir waves. Melrose, Dulk, and Smerd (1978) calculated the degree of polarisation for the harmonic emission for specific Langmuir distributions which modeled realistic Langmuir wave spectra. This was later corrected (Melrose, Dulk, and Gary, 1980) after it had been discovered that important terms had been neglected (Zlotnik, 1981). They concluded that o -mode emission is favoured provided that the Langmuir waves are strongly collimated in the magnetic field direction. An isotropic

spectrum of Langmuir waves favours x -mode emission. In the limit where all the Langmuir waves have wave vectors parallel to the magnetic field, the degree of circular polarisation (in favour of the o -mode) has the simple form (Melrose, Dulk, and Gary, 1980)

$$r_H \approx \frac{11 |\cos \chi| \Omega_e}{48 \omega_p}, \quad (1)$$

where χ is the angle of emission, relative to the magnetic field direction. Hence, there is a direct linear relationship between r_H and Ω_e/ω_p , assuming that the maximum power is radiated at $\theta \approx 45^\circ$ for second harmonic emission. As the observed frequency is at twice the plasma frequency, an observed value of r_H directly gives a value for Ω_e , and hence for the coronal magnetic field strength. For example, a typical value of r_H at 100 MHz is $r_H = 0.10$ (see Figure 1), which yields $B \approx 10^{-3}$ T. Such values for the coronal magnetic field are considerably higher than predicted by other indirect methods (e.g., Dulk and McLean, 1978). For $r_H = 0.20$, observed at frequencies around 435 MHz (Mercier, 1990), $\Omega_e/\omega_p \approx 1.2$. For such high observed values of r_H , the use of the weak-field limit ($\Omega_e \ll \omega_p$) is not justified.

In this paper, we calculate the exact emission rate for the process $Z' + Z'' \rightarrow X, O$, where two z -mode waves (Z', Z'') coalesce to produce a second harmonic x -mode (X) or o -mode (O) wave, assuming neither of the simplifying approximations. In a magnetised plasma, z -mode waves near the z -mode resonance frequency are the counterpart of Langmuir waves in an unmagnetised plasma. Both the magnetic and thermal contributions can be included in an approximate way; for example, in the weak-field limit ($\Omega_e \ll \omega_p$), an approximate dispersion relation for magnetised Langmuir waves is (Melrose, 1986, p. 172)

$$\omega_L^2 \approx \omega_p^2 + 3k_L^2 V_e^2 + \Omega_e^2 \sin^2 \theta. \quad (2)$$

However, in this paper we ignore the thermal correction and use the cold plasma expression for the dispersion relation of the z -mode waves. After taking the unmagnetised limit of the results obtained in this paper, the results for the unmagnetised process $L' + L'' \rightarrow T$ (Willes, Robinson, and Melrose, 1996) are not recovered. This is because the Langmuir wave dispersion relation, $\omega_L(\mathbf{k}_L) \approx \omega_p(1 + 3k_L^2 V_e^2/2\omega_p^2)$ depends on the thermal electron velocity V_e . Further generalisation of this theory would involve including thermal corrections in the magnetised Langmuir waves. The degree of circular polarisation is determined from the relative emission rates for second harmonic x -mode and o -mode waves. In our calculations, we assume physically realistic Langmuir wave number spectra, comprising beam-driven and backscattered components. In Section 2, the properties of the magnetoionic modes are reviewed. The emission rate for the process $Z' + Z'' \rightarrow X, O$ is derived in Section 3. In Section 4.1, we verify the simple relation (1) for the degree of polarisation

in the weak-field limit and where the head-on approximation is assumed. In Section 4.2, we investigate the effects of relaxing these simplifying approximations, and in Section 5, we discuss our results and the implications for the prediction of coronal magnetic field strengths from polarisation measurements.

2. The Magnetoionic Modes

In this section we summarise the properties of the magnetoionic modes in a cold plasma; these are the wave modes in a magnetised plasma in the limit as the electron temperature T_e approaches zero. The magnetoionic modes consist of extraordinary and ordinary modes. The sense of rotation of the electric field vector for extraordinary waves in the plane perpendicular to the magnetic field direction is the same as that for a gyrating electron; for ordinary waves, it is opposite. In the following analysis, the polarisation vector for a magnetoionic wave is expressed in the form (Melrose, 1986, p. 168)

$$\mathbf{e}_\sigma = \frac{L_\sigma \boldsymbol{\kappa} + T_\sigma \mathbf{t} + i \mathbf{a}}{(L_\sigma^2 + T_\sigma^2 + 1)^{1/2}}, \quad (3)$$

where $\sigma = 1$ for the ordinary mode and $\sigma = -1$ for the extraordinary mode, $\boldsymbol{\kappa} = (\sin \theta \cos \phi, \sin \theta \sin \phi, \cos \theta)$, $\mathbf{t} = (\cos \theta \cos \phi, \cos \theta \sin \phi, -\sin \theta)$, $\mathbf{a} = (-\sin \phi, \cos \phi, 0)$, and the magnetic field direction $\mathbf{b} = (0, 0, 1)$. Hence L is the longitudinal component of the polarisation vector (along the magnetic field) and T is the axial ratio of the polarisation ellipse (the path of the electric field vector in the plane perpendicular to the magnetic field direction). The axial ratio T_σ has the form (Melrose, 1986, p. 172)

$$T_\sigma = \frac{Y(1-X)\cos\theta}{\frac{1}{2}Y^2\sin^2\theta - \sigma\Delta} = \frac{-\frac{1}{2}Y^2\sin^2\theta - \sigma\Delta}{Y(1-X)\cos\theta}, \quad (4)$$

with

$$\Delta^2 = \frac{1}{4}Y^4\sin^4\theta + (1-X)^2Y^2\cos^2\theta, \quad (5)$$

and

$$X = \frac{\omega_p^2}{\omega^2}, \quad Y = \frac{\Omega_e}{\omega}. \quad (6)$$

In addition, $T_x T_o = -1$; i.e., the ellipses for the two modes are orthogonal. The longitudinal component L_σ satisfies

$$L_\sigma = \frac{XY\sin\theta}{1-X} \frac{T_\sigma}{T_\sigma - Y\cos\theta} = \frac{XY\sin\theta(1+YT\cos\theta)}{1-X-Y^2+XY^2\cos^2\theta}. \quad (7)$$

The refractive index n_σ satisfies

$$n_\sigma^2 = 1 - \frac{XT_\sigma}{T_\sigma - Y \cos \theta} = 1 - \frac{X(1-X)(1+YT \cos \theta)}{1-X-Y^2+XY^2 \cos^2 \theta}. \quad (8)$$

The ratio of electric to total energy in magnetoionic waves satisfies

$$R_\sigma = \frac{L_\sigma^2 + T_\sigma^2 + 1}{T_\sigma^2 + 1} \frac{1}{2n_\sigma \partial(\omega n_\sigma) / \partial \omega}. \quad (9)$$

The two alternative forms given in (4), (7), and (8) are necessary to avoid (unphysical) singularities in numerical calculations. Figure 2 illustrates the magnetoionic mode dispersion relation (n^2 against ω) for the extraordinary (solid line) and ordinary (dashed line) modes, for (a) $\omega_p = \Omega_e/2$, $\theta = 0$, (b) $\omega_p = 2\Omega_e$, $\theta = 0$, (c) $\omega_p = \Omega_e/2$, $\theta = \pi/20$, (d) $\omega_p = 2\Omega_e$, $\theta = \pi/20$, (e) $\omega_p = \Omega_e/2$, $\theta = \pi/2$, and (f) $\omega_p = 2\Omega_e$, $\theta = \pi/2$. The higher frequency components of the ordinary and extraordinary modes are referred to here as the o -mode and the x -mode, respectively. The cutoffs occur at

$$\omega_o = \omega_p, \quad (10)$$

for the o -mode and

$$\omega_x = \frac{\Omega_e + (\Omega_e^2 + 4\omega_p^2)^{1/2}}{2}, \quad (11)$$

for the x -mode, and are labelled in Figure 2(e). Both the x - and o -modes asymptote to $n^2 = 1$ at high frequencies. Away from the cutoffs, both the x - and o -modes are transverse and circularly polarised. The lower frequency extraordinary mode component is named the z -mode. The cutoff for the z -mode occurs at

$$\omega_{zc} = \omega_x - \Omega_e = \frac{-\Omega_e + (\Omega_e^2 + 4\omega_p^2)^{1/2}}{2}. \quad (12)$$

The resonance for the z -mode occurs at

$$\omega_{zr} = \left\{ \frac{(\omega_p^2 + \Omega_e^2) + [(\omega_p^2 + \Omega_e^2)^2 - 4\omega_p^2 \Omega_e^2 \cos^2 \theta]^{1/2}}{2} \right\}^{1/2}, \quad (13)$$

and is angle dependent. As a result, the z -mode resonance occurs in the frequency range $\omega_{zr-} \leq \omega \leq \omega_{zr+}$ with, for $\theta = 0$,

$$\omega_{zr-} = \left\{ \frac{(\omega_p^2 + \Omega_e^2) + [(\omega_p^2 + \Omega_e^2)^2 - 4\omega_p^2 \Omega_e^2]^{1/2}}{2} \right\}^{1/2}, \quad (14)$$

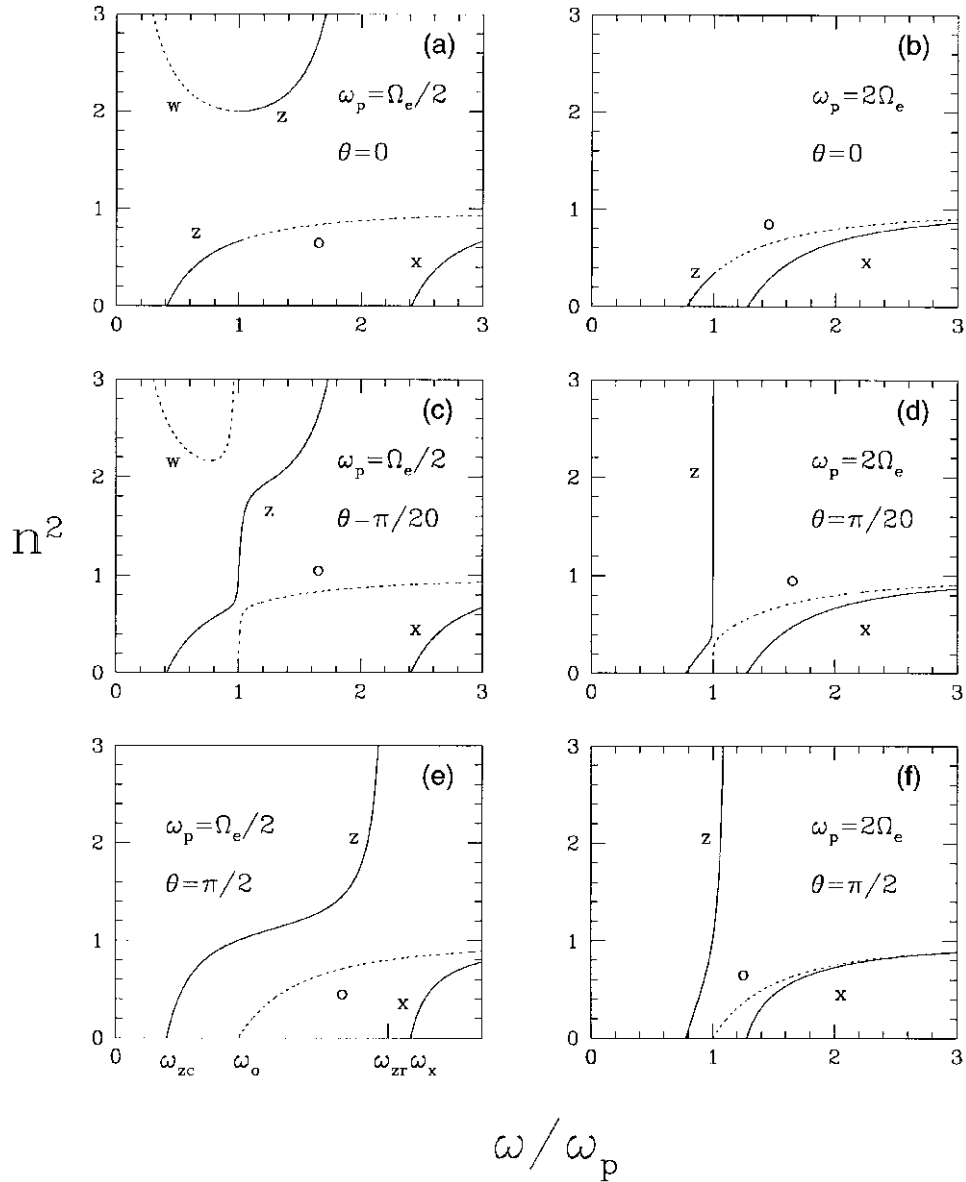


Figure 2. Dispersion relation (n^2 against ω) for magnetoionic waves for (a) $\omega_p = \Omega_e/2$, $\theta = 0$, (b) $\omega_p = 2\Omega_e$, $\theta = 0$, (c) $\omega_p = \Omega_e/2$, $\theta = \pi/20$, (d) $\omega_p = 2\Omega_e$, $\theta = \pi/20$, (e) $\omega_p = \Omega_e/2$, $\theta = \pi/2$, and (f) $\omega_p = 2\Omega_e$, $\theta = \pi/2$. The modes are labelled w (whistler mode), o (o -mode), z (z -mode), and x (x -mode). The cutoff and resonance frequencies ω_{zc} (cutoff for z -mode), ω_{zr} (resonance for z -mode), ω_o (cutoff for o -mode), and ω_x (cutoff for x -mode) are labelled in frame (e).

and, for $\theta = \pi/2$,

$$\omega_{zT+} = (\omega_p^2 + \Omega_e^2)^{1/2}. \quad (15)$$

Note that at $\theta = 0$ (Figures 2(a) and 2(b)), the z - and o -modes join at $\omega = \omega_p$. At high values of n^2 , in the vicinity of the z -mode resonance, the z -mode waves are predominantly longitudinal.

In Section 3, we derive the emission rate for the process $Z' + Z'' \rightarrow X, O$, where two z -mode waves (Z' and Z'') coalesce to produce an x -mode wave (X) or an o -mode wave (O). In Section 4, the emission rates for the two processes $Z' + Z'' \rightarrow X$ and $Z' + Z'' \rightarrow O$ are compared to determine the degree of circular polarisation. In the unmagnetised limit ($\Omega_e/\omega_p \rightarrow 0$), the dispersion relation for both the x - and o -modes approaches that for transverse waves in an unmagnetised plasma (with opposite senses of circular polarisation, and dispersion relation $n^2 = 1 - \omega_p^2/\omega^2$), and the z -mode dispersion relation approaches that for Langmuir waves (without thermal effects).

3. Second Harmonic Emission Rate: $Z' + Z'' \rightarrow X, O$

In this section we derive an expression for the second harmonic emission rate for x -mode and o -mode waves. Evaluation of the emission rate requires two-dimensional numerical integration, and the evaluation of the integrand requires iterative numerical techniques, which are summarised in the Appendix.

We proceed in a similar manner to a derivation of the emission rate for the unmagnetised process $L' + L'' \rightarrow T$ (Willes, Robinson, and Melrose, 1996). The second harmonic emission rate for the process $Z'(\mathbf{k}') + Z''(\mathbf{k}'') \rightarrow T(\mathbf{k})$, for $T = X$ or O , is of the form (Melrose and Sy, 1972)

$$\frac{dT_T(\mathbf{k})}{dt} = \frac{2}{\hbar\omega_p} \int \frac{d^3\mathbf{k}'}{(2\pi)^3} \int \frac{d^3\mathbf{k}''}{(2\pi)^3} u_{TZZ}(\mathbf{k}, \mathbf{k}', \mathbf{k}'') T_Z(\mathbf{k}') T_Z(\mathbf{k}''), \quad (16)$$

where T_Z is the effective temperature of the z -mode waves, and T_T is the effective (brightness) temperature of the transverse waves. In this equation, terms proportional to $T_T(\mathbf{k}) T_Z(\mathbf{k}')$ and $T_T(\mathbf{k}) T_Z(\mathbf{k}'')$ are omitted. This is a valid assumption provided the wave levels of transverse waves remain well below the z -mode waves; i.e., the process does not saturate. The probability for the three wave process $Z' + Z'' \rightarrow T$ has the form

$$\begin{aligned} u_{TZZ}(\mathbf{k}, \mathbf{k}', \mathbf{k}'') &= \frac{4\hbar R_T(\mathbf{k}) R_Z(\mathbf{k}') R_Z(\mathbf{k}'')}{\epsilon_0^3 \omega_T(\mathbf{k}) \omega_Z(\mathbf{k}') \omega_Z(\mathbf{k}'')} |\alpha_{TZZ}(\mathbf{k}, \mathbf{k}', \mathbf{k}'')|^2 \times \\ &\times (2\pi)^4 \delta^3(\mathbf{k} - \mathbf{k}' - \mathbf{k}'') \delta(\omega - \omega' - \omega''), \end{aligned} \quad (17)$$

with

$$\alpha_{TZZ}(\mathbf{k}, \mathbf{k}', \mathbf{k}'') = e_{Ti}^*(\mathbf{k})e_{Zj}(\mathbf{k}')e_{Zl}(\mathbf{k}'')\alpha_{ijl}(\mathbf{k}, \mathbf{k}', \mathbf{k}'') ,$$

and $\omega = \omega_T(\mathbf{k})$, $\omega' = \omega_Z(\mathbf{k}')$, and $\omega'' = \omega_Z(\mathbf{k}'')$. The subscripts i , j , and l refer to vector elements of \mathbf{e} and tensor elements of α . The quadratic nonlinear response tensor α_{ijl} satisfies (Melrose, 1986, p. 165)

$$\begin{aligned} \alpha_{ijl}(\mathbf{k}, \mathbf{k}', \mathbf{k}'') = & -\frac{e^3 n_e}{2m_e^2} \left[\frac{k_r \tau_{rj}(\omega') \tau_{il}(\omega'')}{\omega'} + \frac{k_r \tau_{rl}(\omega'') \tau_{ij}(\omega')}{\omega''} + \right. \\ & + \frac{k_r' \tau_{ir}(\omega) \tau_{jl}(\omega'')}{\omega} + \frac{k_r'' \tau_{ir}(\omega) \tau_{lj}(\omega')}{\omega} - \\ & \left. - \frac{k_r'' \tau_{rj}(\omega') \tau_{il}(\omega)}{\omega'} - \frac{k_r' \tau_{rl}(\omega'') \tau_{ij}(\omega)}{\omega''} \right] , \end{aligned} \quad (19)$$

with

$$\tau_{ij}(\omega) = \frac{\omega^2 \delta_{ij} - \Omega_e^2 b_i b_j - i\omega \Omega_e \varepsilon_{ijk} b_k}{\omega^2 - \Omega_e^2} , \quad (20)$$

for $\mathbf{b} = \mathbf{B}/|\mathbf{B}|$.

For the magnetoionic modes, the expression (18) is simplified with the aid of the wave equation for magnetoionic waves,

$$\left[n^2(\kappa_i \kappa_j - \delta_{ij}) + \delta_{ij} - \frac{\omega_p^2}{\omega^2} \tau_{ij} \omega \right] e_j = 0 , \quad (21)$$

which implies

$$\tau_{ij}(\omega) e_j = f_i \quad (22)$$

for

$$\mathbf{f} := \frac{\omega_p^2}{\omega^2} [\mathbf{e} - n^2(\mathbf{e} - \boldsymbol{\kappa} \boldsymbol{\kappa} \cdot \mathbf{e})] . \quad (23)$$

Thus, (18) becomes

$$\begin{aligned} \alpha_{TZZ}(\mathbf{k}, \mathbf{k}', \mathbf{k}'') = & \left[\frac{\mathbf{k} \cdot \mathbf{f}'_Z \mathbf{e}_T^* \cdot \mathbf{f}''_Z}{\omega'} + \frac{\mathbf{k} \cdot \mathbf{f}''_Z \mathbf{e}_T^* \cdot \mathbf{f}'_Z}{\omega''} + \frac{\mathbf{k}' \cdot \mathbf{f}_T^* \mathbf{e}'_Z \cdot \mathbf{f}''_Z}{\omega} + \right. \\ & \left. + \frac{\mathbf{k}'' \cdot \mathbf{f}_T^* \mathbf{e}''_Z \cdot \mathbf{f}'_Z}{\omega} - \frac{\mathbf{k}'' \cdot \mathbf{f}'_Z \mathbf{f}_T^* \cdot \mathbf{e}''_Z}{\omega'} - \frac{\mathbf{k}' \cdot \mathbf{f}''_Z \mathbf{f}_T^* \cdot \mathbf{e}'_Z}{\omega''} \right] , \end{aligned} \quad (24)$$

where the prefactor of physical constants common to both the x - and o -modes is omitted. From (3), the polarisation vector \mathbf{e}_σ may be expressed in the form

$$\mathbf{e}_\sigma = (a_\sigma \cos \phi - i \sin \phi, a_\sigma \sin \phi + i \cos \phi, b_\sigma), \quad (25)$$

with

$$a_\sigma = \frac{L_\sigma \sin \theta + T_\sigma \cos \theta}{(L_\sigma^2 + T_\sigma^2 + 1)^{1/2}}, \quad (26)$$

$$b_\sigma = \frac{L_\sigma \cos \theta - T_\sigma \sin \theta}{(L_\sigma^2 + T_\sigma^2 + 1)^{1/2}}. \quad (27)$$

Similarly, \mathbf{f}_σ may be expressed as

$$\mathbf{f}_\sigma = (g_\sigma \cos \phi - ih_\sigma \sin \phi, g_\sigma \sin \phi + ih_\sigma \cos \phi, b_\sigma), \quad (28)$$

with

$$g_\sigma = \frac{L_\sigma \sin \theta + (1 - n_\sigma^2)T_\sigma \cos \theta}{X(L_\sigma^2 + T_\sigma^2 + 1)^{1/2}}, \quad (29)$$

$$h_\sigma = \frac{1 - n_\sigma^2}{X(L_\sigma^2 + T_\sigma^2 + 1)^{1/2}}. \quad (30)$$

We now focus our attention on the evaluation of the integral (16) for a given functional form for the wave number spectrum of coalescing z -mode waves. We proceed as for the derivation of the unmagnetised emission rate (Willes, Robinson, and Melrose, 1996), but due to the greater complexity of the integrand, the integral (16) is reduced to two dimensions and is evaluated numerically (in Willes, Robinson, and Melrose (1996) it is a one-dimensional integral, which may be further simplified to an analytic expression by adopting the ‘narrow-spectrum’ approximation). The integral over $d^3\mathbf{k}''$ is evaluated using the delta function over wave vectors, with $\mathbf{k}'' = \mathbf{k} - \mathbf{k}'$. The remaining integral is decomposed into radial and angular components,

$$\int d^3\mathbf{k}' = \int_0^\infty dk' k'^2 \int_0^\pi d\theta' \sin \theta' \int_{-\pi}^\pi d\phi', \quad (31)$$

and the dk' integral is evaluated using the delta function over wave frequencies in (17), using the relation

$$\int dk' f(k') \delta[g(k')] = \frac{f(k'_0)}{|g'(k'_0)|} \quad (32)$$

for

$$g(k') = \omega_T(\mathbf{k}) - \omega_Z(\mathbf{k}') - \omega_Z(\mathbf{k} - \mathbf{k}'), \quad (33)$$

and where $g'(k')$ is the derivative of $g(k')$ with respect to k' . The remaining integrand of (16) is represented by $f(k')$, and k'_0 is the (sole) value of k' at which $g(k') = 0$. The final form of (16) to be evaluated numerically is

$$\begin{aligned} \frac{dT_T(\mathbf{k})}{dt} = & \int_0^\pi d\theta' \int_{-\pi}^\pi d\phi' \frac{\sin \theta' k_0'^2 R_T(\mathbf{k}) R_Z(k'_0) R_Z(\mathbf{k}''_0)}{|g'(k'_0)| \omega_T(\mathbf{k}) \omega_Z(\mathbf{k}'_0) \omega_Z(\mathbf{k}''_0)} \times \\ & \times |\alpha_{TZZ}(\mathbf{k}, \mathbf{k}'_0, \mathbf{k}''_0)|^2 T_Z(\mathbf{k}'_0) T_Z(\mathbf{k}''_0), \end{aligned} \quad (34)$$

where R_T and R_Z are evaluated from (9), ω_T and ω_Z from (8), and α_{TZZ} from (24). \mathbf{k}'_0 and \mathbf{k}''_0 are the values of \mathbf{k}' and $\mathbf{k}'' = \mathbf{k} - \mathbf{k}'$ at which $g(k') = 0$. The prefactor common to both the x - and o -mode emission rates has been omitted in (34) because we are concerned only with the relative x - and o -mode emission rates. The procedure for numerically evaluating (34) is summarised in the Appendix.

In evaluating the emission rate (34), we assume a Gaussian wave-number spectrum for the coalescing z -mode waves (Willes, Robinson, and Melrose, 1996). The Gaussian spectrum consists of a forward component, which peaks at wave numbers parallel to \mathbf{B} , with $k_{\parallel} = k_f$, and a backward component, which peaks at $k_{\parallel} = k_b$ (typically, $k_b < 0$). The forward and backward components model the beam-driven and backscattered z -mode waves. The Gaussian spectrum has the form

$$\begin{aligned} T_Z(\mathbf{k}) = & \xi T_f \exp \left[\frac{-(k_{\parallel} - k_f)^2 - k_{\perp}^2}{K_f^2} \right] + \\ & + (1 - \xi) T_b \exp \left[\frac{-(k_{\parallel} - k_b)^2 - k_{\perp}^2}{K_b^2} \right], \end{aligned} \quad (35)$$

where T_f and T_b are normalisation coefficients, K_f is the characteristic width of the forward component, K_b is the characteristic width of the backward component, and $0 \leq \xi \leq 1$ is the fractional energy in the forward component (assumed here to be $\xi = 0.5$). The angular distribution of z -mode waves thus strongly peaks about $\theta = 0$ and π . As a result, high wave number z -mode waves have wave frequencies close to ω_{zr-} . The frequency range of product transverse (o - or x -mode) waves from the coalescence of two z -mode waves satisfies (with $\omega_T = \omega'_Z + \omega''_Z$)

$$2\omega_{zr-} \leq \omega_T \lesssim 2\omega_{\text{upper}} \ll 2\omega_{zr+}, \quad (36)$$

where ω_{upper} is obtained by substituting the value for θ near the edge of the forward component of the z -mode spectrum θ_{upper} into (13). Figure 3 illustrates how θ_{upper} is obtained, with

$$\cos \theta_{\text{upper}} = \frac{k_f}{(k_f^2 + K_f^2)^{1/2}}. \quad (37)$$

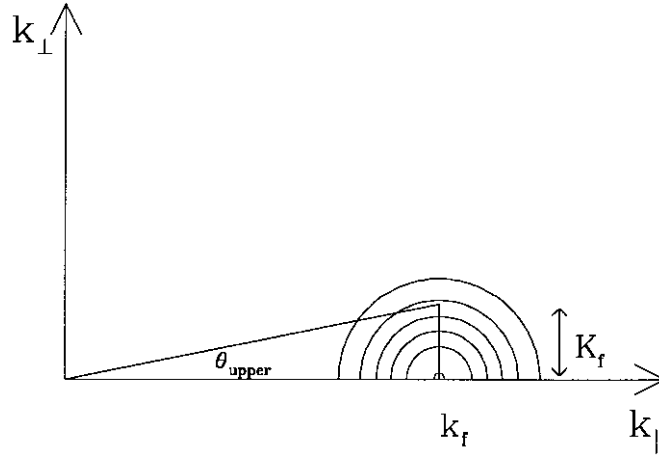


Figure 3. The angle $\theta_{\text{upper}} = \cos^{-1}[k_f/(k_f^2 + K_f^2)^{1/2}]$ determines the approximate upper frequency ω_{upper} of the z -mode waves in the forward component of the z -mode wave number spectrum.

This gives

$$\omega_{\text{upper}} = \left\{ \frac{(\omega_p^2 + \Omega_e^2) + [(\omega_p^2 + \Omega_e^2)^2 - 4\omega_p^2\Omega_e^2k_f^2/(k_f^2 + K_f^2)]^{1/2}}{2} \right\}^{1/2}. \quad (38)$$

We are concerned only with second harmonic waves in the frequency range (36), and so define the dimensionless frequency δ , with

$$\delta(\omega_T) := \frac{\omega_T - 2\omega_{zr-}}{2\omega_{\text{upper}} - 2\omega_{zr-}}. \quad (39)$$

Hence, $\delta = 0$ for $\omega_T = 2\omega_{zr-}$ and $\delta = 1$ for $\omega_T = 2\omega_{\text{upper}}$.

4. Results

The degree of polarisation r is defined by (Melrose and Sy, 1972)

$$r(\mathbf{k}) := \frac{dT_o(\mathbf{k})/dt - dT_x(\mathbf{k})/dt}{dT_o(\mathbf{k})/dt + dT_x(\mathbf{k})/dt}, \quad (40)$$

with the emission rate $dT_T(\mathbf{k})/dt$ given by (34). For fully o -mode emission, $r = 1$, and for fully x -mode emission, $r = -1$. We first verify the simple expression (1), where the head-on and weak-field approximations are assumed (Section 4.1) before relaxing these simplifying approximations (Section 4.2).

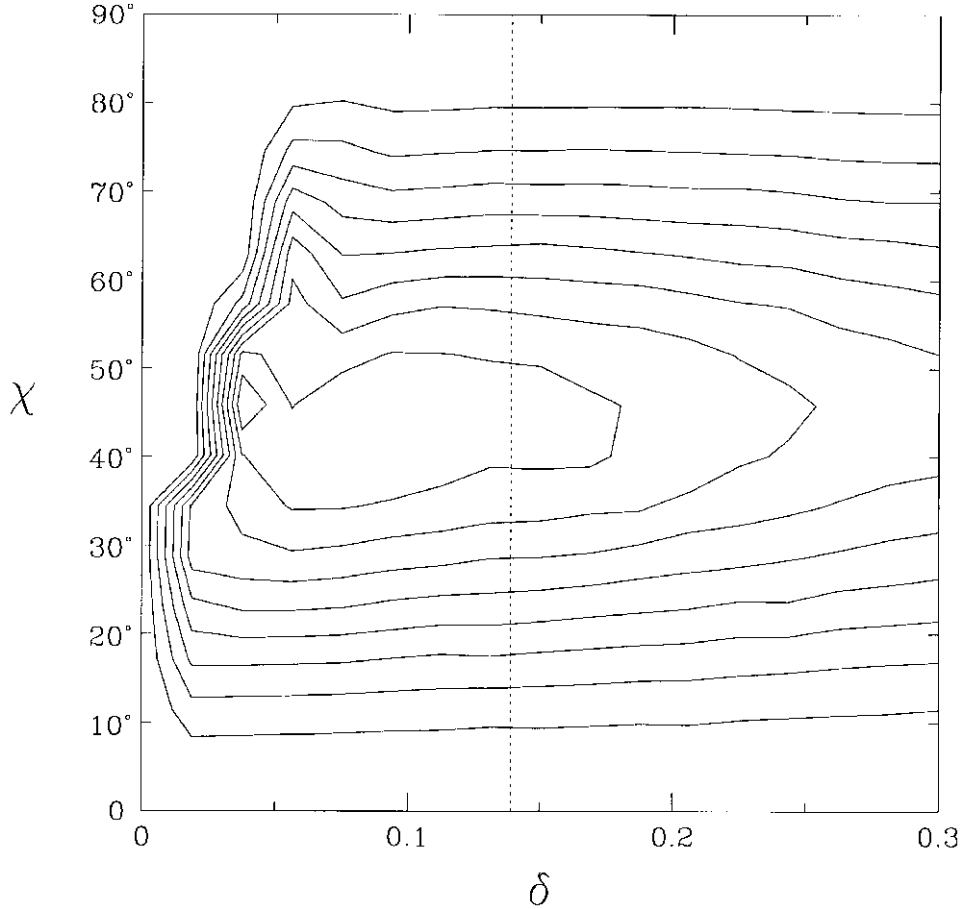


Figure 4. Contours of o -mode emission rate, as a function of emission angle χ and dimensionless frequency δ , for $k_f = -k_b = 20k_T$, $K_f = K_b = 0.1k_f$, and $\Omega_e/\omega_p = 0.2$. The contour levels vary linearly from zero to the maximum value.

4.1. HEAD-ON AND WEAK-FIELD APPROXIMATIONS

After taking the weak-field limit ($\Omega_e/\omega_p \rightarrow 0$) and assuming the head-on approximation ($|k_f|, |k_b| \gg k_T$) for z -mode waves collimated along the magnetic field direction (valid for Gaussian spectra with $|K_f/k_f|, |K_b/k_b| \ll 1$), the degree of polarisation satisfies (1). We verify that our results are consistent with (1) for Gaussian z -mode spectra for which the head-on approximation ($k_f = -k_b = 20k_T \gg k_T$) and the weak-field limit ($\Omega_e/\omega_p = 0.2 \ll 1$) are valid, and where the spectra are confined to a narrow range of angles close to the magnetic field direction ($K_f = K_b = 0.1k_f$).

Figure 4 displays the o -mode emission rate as contours over the range of angles $0 \leq \chi \leq 90^\circ$ and (dimensionless) o -mode wave frequencies in the range $\delta = 0$

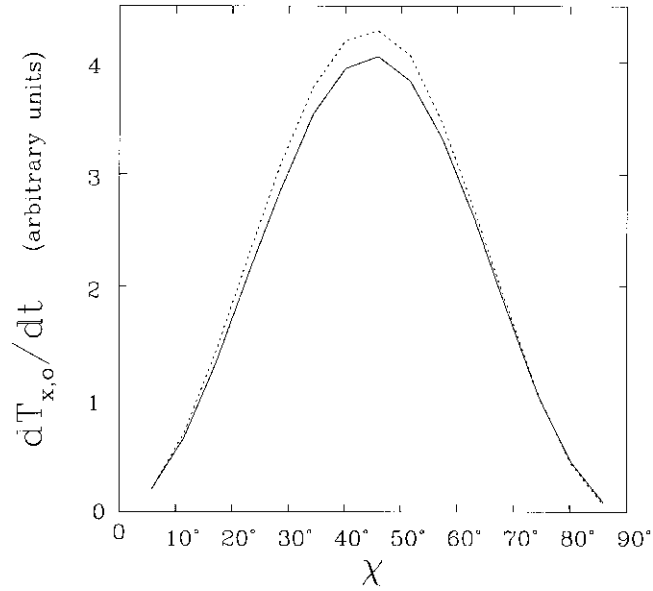


Figure 5. *x*-mode (solid line) and *o*-mode (dashed line) emission rates as a function of emission angle χ , at frequency $\delta = 0.14$ (dashed line) in Figure 4.

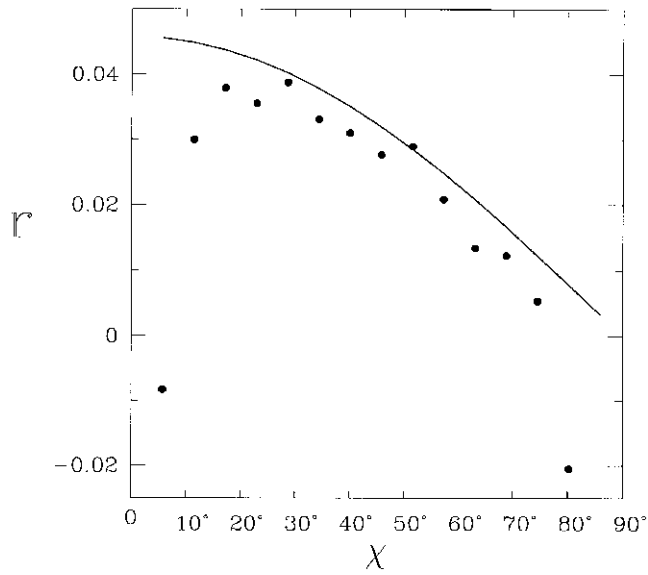


Figure 6. Degree of polarisation r as a function of emission angle χ for the *x*-mode and *o*-mode emission rates in Figure 5 (dots) and after assuming the head-on and weak-field approximations (solid line).

to 0.3. A similar plot can also be produced for the x -mode emission rate. Computational limitations do not permit us to accurately calculate r over the full range shown in Figure 4. Nevertheless, the essential behaviour of r can be determined by taking a vertical slice through Figure 4; i.e., by fixing δ , and plotting the emission rate against emission angle χ . Figure 5 shows one such slice for $\delta = 0.14$, represented by the dashed line in Figure 4. The solid line in Figure 5 represents the x -mode emission rate and the dashed line represents the o -mode emission rate. Figure 6 shows the corresponding degree of polarisation r (40) as a function of emission angle χ for the o -mode and x -mode emission rates shown in Figure 5. The solid line represents the degree of polarisation assuming the head-on and weak-field approximations (1), and the dots represent the degree of polarisation for the parameters $k_f = -k_b = 20k_T$, $K_f = K_b = 0.1k_f$, and $\Omega_e/\omega_p = 0.2$. Due to slow convergence of the numerical integration in this limit, the dots in Figure 6 typically have an associated error of approximately 10%. The agreement is reasonably good between the approximate and exact values for r , except in a small range of angles about $\chi = 0^\circ$ and 90° , where r is negative (favouring x -mode polarisation). This is a consequence of the finite width of the Langmuir wave spectra. The exact case (points) assumes spectral widths $K_f = K_b = 0.1k_f$, whereas the approximation (1) is obtained by assuming Langmuir waves parallel to the magnetic field lines, with zero width. In the limit as $K_f/k_f, K_b/k_b \rightarrow 0$, closer agreement is achieved. Over the remainder of emission angles, the exact and approximate values for r agree to within 20%. This is consistent with the next order term in (1) being of order Ω_e/ω_p ($\approx 20\%$) times the smallest terms retained.

4.2. RELAXATION OF SIMPLIFYING APPROXIMATIONS

We now consider the effects of relaxing the head-on and weak-field approximations. We first consider the results for parameters in the regime where the head-on approximation begins to break down, with $k_f = -k_b = 5k_T$, and $K_f = K_b = 0.2k_f$, and where the weak-field limit ($\Omega_e/\omega_p \ll 1$) is invalid, with $\Omega_e/\omega_p = 0.8$. The spectral parameters k_f and K_f are related to the electron beam speed and width, with (e.g., Robinson, Willes, and Cairns, 1993) $k_f \approx \omega_p/v_{\text{beam}}$ and $K_f/k_f \approx \Delta v_{\text{beam}}/v_{\text{beam}}$. Hence, the chosen spectral parameters correspond to type III parameters $v_{\text{beam}} \approx 0.12c$ and $\Delta v_{\text{beam}}/v_{\text{beam}} \approx 0.2$. We later consider results for faster beam speeds (and hence lower beam wave numbers) where the head-on approximation becomes increasingly less well satisfied.

Figure 7 shows contours of the o -mode emission rate as a function of emission angle χ and dimensionless frequency δ (for $0 \leq \delta \leq 0.4$). Figure 8 displays the x - and o -mode emission rates as a function of χ for $\delta = 0.2$ (the dashed line in Figure 4.2). Figure 9 plots the degree of polarisation (dots) for the x - and o -mode emission rates shown in Figure 8. o -mode polarisation is favoured at the peak of emission (about $\chi = 45^\circ$) and hence is more likely to be observed. More x -mode emission (negative r) is produced than predicted when the head-on and weak-field

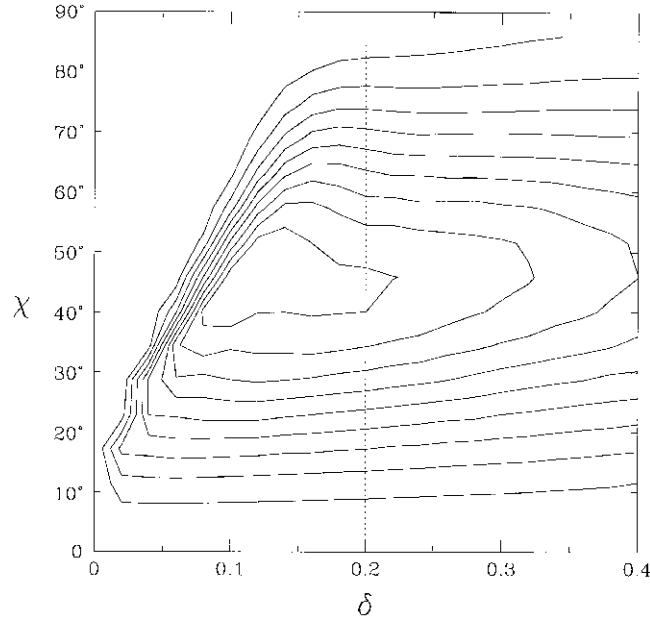


Figure 7. Contours of *o*-mode emission rate, as a function of emission angle χ and dimensionless frequency δ , for $k_f = -k_b = 5k_T$, $K_f = K_b = 0.2k_f$, and $\Omega_e/\omega_p = 0.8$. The contour levels vary linearly from zero to the maximum value.

approximations are assumed (solid line). The important point to note is that, in general, lower values of r are predicted than from (1).

We now consider the more physically realistic situation where the backscattered *z*-mode waves are produced at lower wave numbers, with offset k_0 , such that $\mathbf{k}_b = \mathbf{k}_0 - \mathbf{k}_f$. The wave number offset k_0 is dependent on the plasma parameters, with (Cairns, 1987)

$$k_0 = \frac{2}{3} \sqrt{\frac{\gamma m_e \omega_p}{m_i V_e}},$$

where m_e and m_i are the electron and ion masses, and $\gamma = 1 + 3T_i/T_e$, with T_e and T_i the electron and ion temperatures. For typical coronal type III burst parameters ($T_i = T_e$, $V_e = 5 \times 10^6 \text{ m s}^{-1}$), $k_0 \approx k_T$. Figure 10 shows the *x*- and *o*-mode emission rates and Figure 11 shows r as a function of χ for the same parameters as for Figures 8 and 9, except with $k_b = -4k_T$ (i.e., with $k_0 = k_T$). In this case, the *o*-mode emission rate is relatively higher than the *x*-mode emission rate than for symmetric spectra (Figures 8 and 9). As a result, higher degrees of polarisation are obtained, closer to the values for r predicted assuming the head-on and weak-field approximations (1). In both cases (symmetric and offset spectra), at the peak emission rate, the condition

$$r \lesssim \frac{11 |\cos \chi| \Omega_e}{48 \omega_p} \quad (42)$$

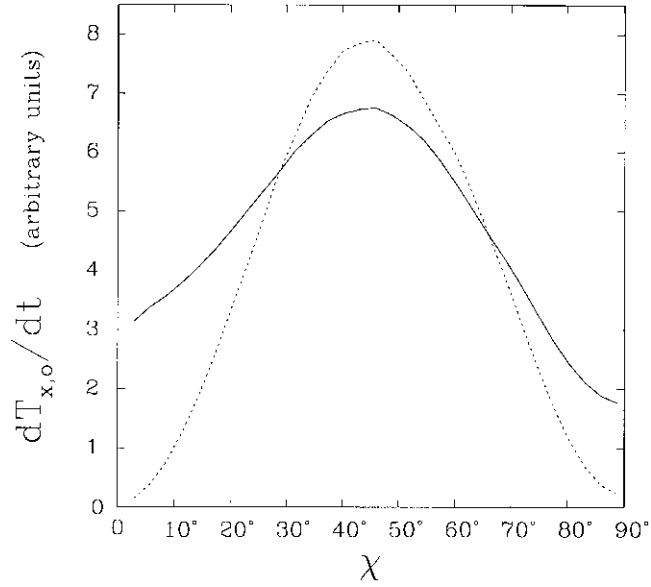


Figure 8. x -mode (solid line) and o -mode (dashed line) emission rates as a function of emission angle χ , at frequency $\delta = 0.2$ (dashed line in Figure 7).

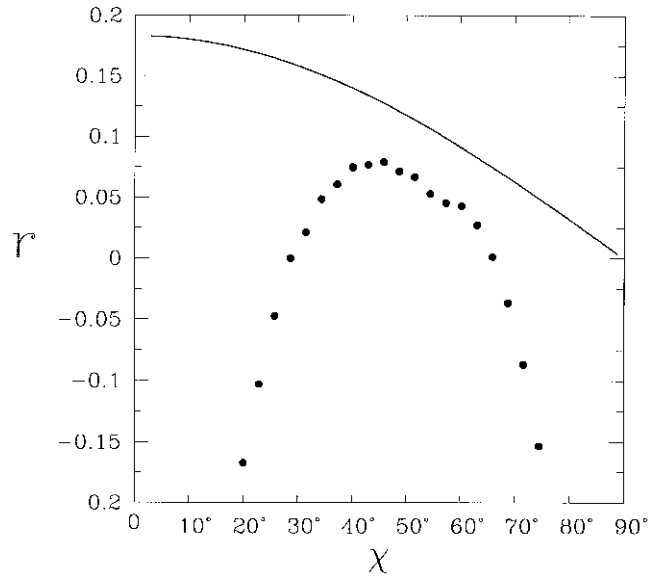


Figure 9. Degree of polarisation r as a function of emission angle χ for the x -mode and o -mode emission rates in Figure 8 (dots) and after assuming the head-on and weak-field approximations (solid line).

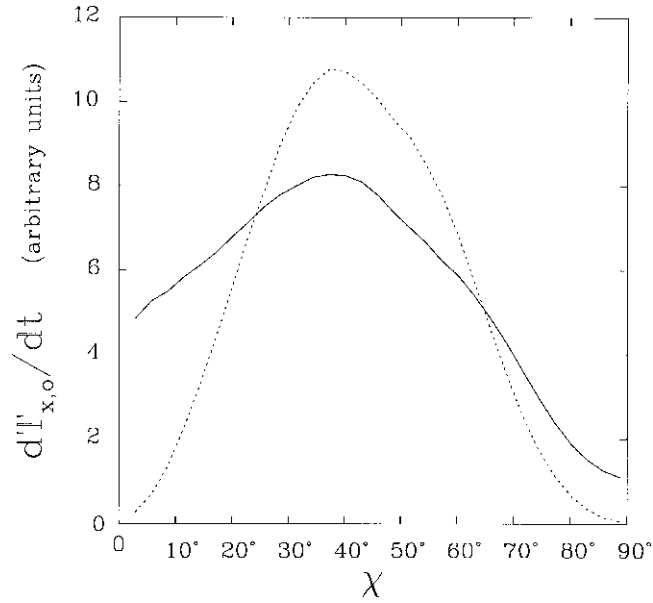


Figure 10. x -mode (solid line) and o -mode (dashed line) emission rates as a function of emission angle χ , at frequency $\delta = 0.2$ for offset backscattered z -mode waves ($k_f = 5k_T$, $k_b = -4k_T$, $K_f = K_b = 0.2k_f$, $\Omega_e/\omega_p = 0.8$).

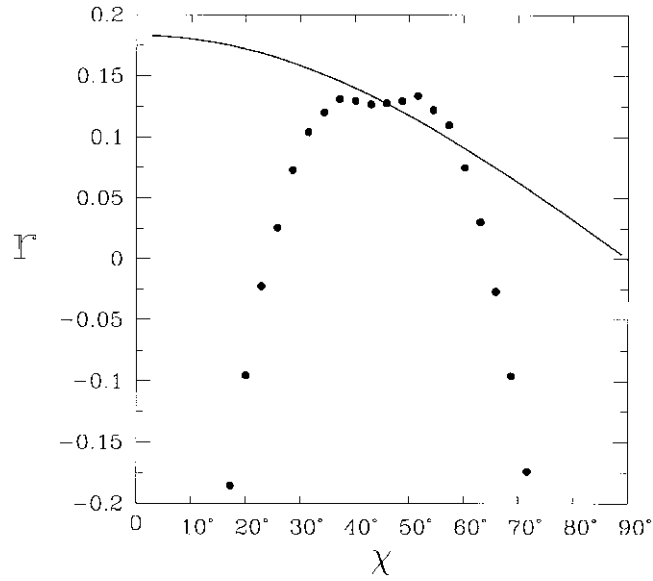


Figure 11. Degree of polarisation r as a function of emission angle χ for the x -mode and o -mode emission rates in Figure 10 (dots) and after assuming the head-on and weak-field approximations (solid line).

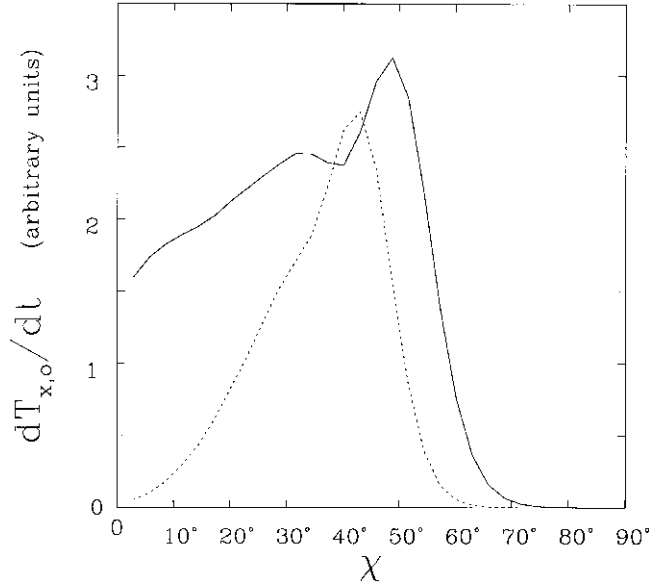


Figure 12. x -mode (solid line) and o -mode (dashed line) emission rates as a function of emission angle χ , at frequency $\delta = 0.5$, for $k_f = -k_b = 2k_T$, $K_f = K_b = 0.2k_f$, $\Omega_e/\omega_p = 0.8$.

is generally satisfied. The parameters chosen for Figures 10 and 11 lie just outside the regime where (42) is satisfied, with values of r slightly above the solid line in Figure 11 predicted at emission angles between 50° and 60° . However, the relation (42) is always satisfied for higher $k_f \gtrsim 5k_T$. The difference between peak values for r for $k_0 = 0$ and $k_0 = k_T$ are even more dramatic for narrower wave number spectra. In effect, a non-zero offset eases the kinematic constraints for the process to proceed. Condition (42) is valid provided that $\Omega_e/\omega_p \lesssim 1$. For $\Omega_e/\omega_p \gtrsim 1$, x -mode emission dominates, with $r \approx -1$.

A different regime applies for even lower Langmuir beam wave numbers (corresponding to higher beam velocities), where the head-on approximation is invalid. Figures 12 and 13 show the second harmonic x - and o -mode emission rates (arbitrary units) and degree of polarisation r as a function of χ , for $k_f = -k_b = 2k_T$ (corresponding to a mean electron beam speed $v_{\text{beam}} \approx 0.3c$), $K_f = K_b = 0.2k_f$, $\Omega_e/\omega_p = 0.8$, and $\delta = 0.5$. For these parameters, x -mode emission dominates over nearly all angles. However, once an offset is introduced in the backscattered z -mode waves ($k_f = 2k_T$, $k_b = -k_T$), o -mode emission dominates, as illustrated in Figures 14 and 15. The emission rate is highest at lower angles (well below $\chi = 45^\circ$). The degree of polarisation r at the peak of emission is significantly higher than predicted by (1) (the solid line in Figure 15). The degree of polarisation at the peak emission rate tends to increase with increasing Ω_e/ω_p , up to $\Omega_e/\omega_p \approx 1$. Again, for $\Omega_e/\omega_p \gtrsim 1$, only x -mode emission is produced (irrespective of the magnitude of the offset in the backscattered Langmuir waves).

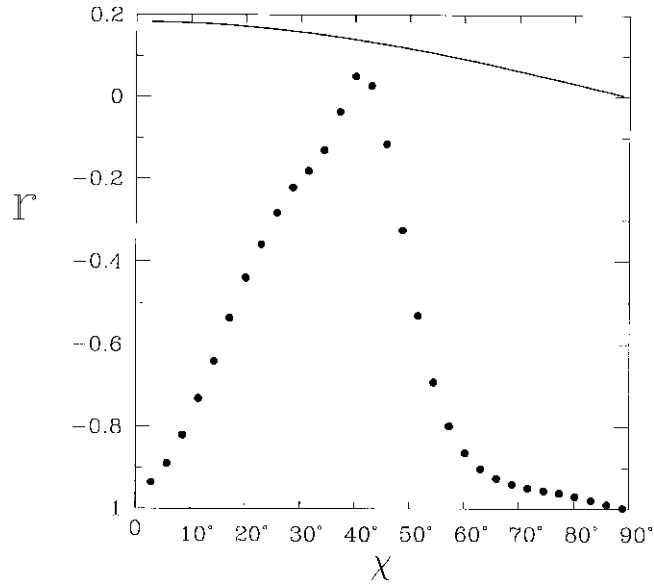


Figure 13. Degree of polarisation r as a function of emission angle χ for the x -mode and o -mode emission rates in Figure 12 (dots) and after assuming the head-on and weak-field approximations (solid line).

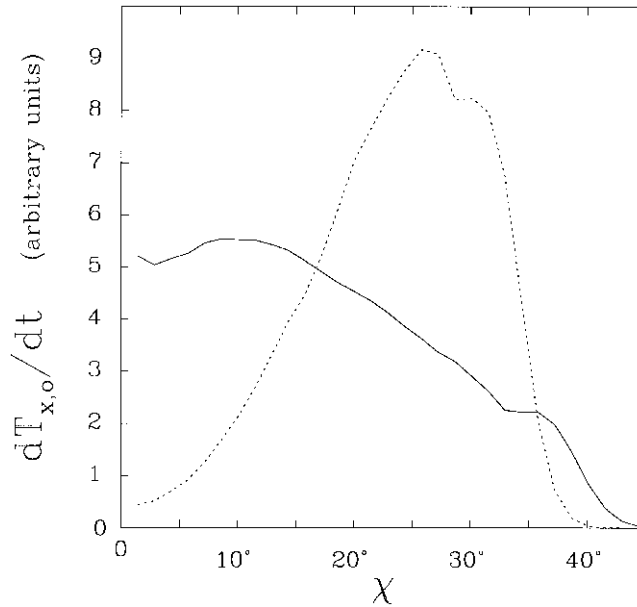


Figure 14. x -mode (solid line) and o -mode (dashed line) emission rates as a function of emission angle χ , at frequency $\delta = 0.5$, for $k_f = 2k_T$, $k_b = -k_T$, $K_f = K_b = 0.2k_f$, $\Omega_e/\omega_p = 0.8$.

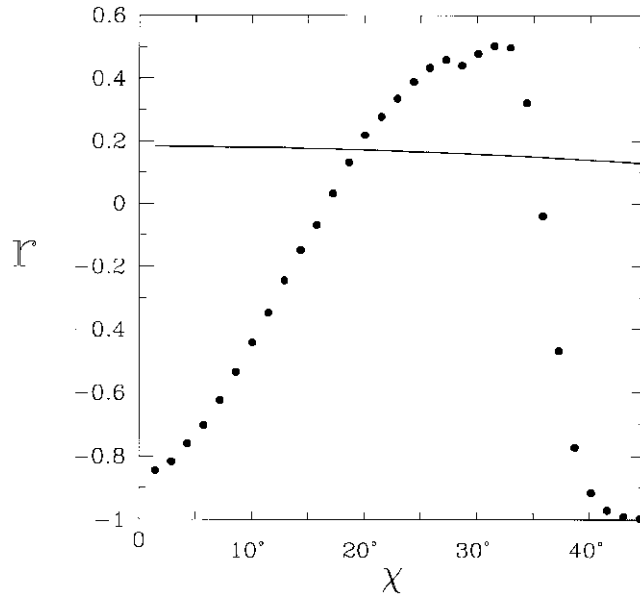


Figure 15. Degree of polarisation r as a function of emission angle χ for the x -mode and o -mode emission rates in Figure 14 (dots) and after assuming the head-on and weak-field approximations (solid line).

5. Discussion

In discussing the above results, two regimes are considered:

(i) For $0 \leq \Omega_e/\omega_p \lesssim 1$, and $k_{\text{beam}} \gg k_T$ (where the head-on approximation is reasonably well satisfied), the predicted degree of polarisation r at the peak emission rate is generally lower than if both the head-on and weak-field approximations are assumed (so that (42) replaces (1)). Higher coronal magnetic fields are predicted using (42) in place of (1). In most cases, o -mode polarisation is favoured at the peak of emission. Predicted values for r strongly depend on the magnitude of the offset between the beam-driven and backscattered Langmuir wave numbers, which depends on the plasma parameters at the source of harmonic type III emission. Our results are consistent with the majority of observed values for r (Dulk and Suzuki, 1980) for harmonic bursts observed in ≈ 700 fundamental-harmonic pairs (see Figure 1). The observed values lie in the range $0 \leq r \lesssim 0.3$, with a strong peak at $r \approx 0.1$. There is ambiguity as to whether the observed emission is polarised in favour of the x -mode or the o -mode. For example, observed left-hand polarised emission is o -mode emission if the magnetic field lines point towards the observer, or x -mode emission if the field lines point away from the observer. However, the observed harmonic emission is very likely to be polarised in favour of the o -mode for two reasons (Dulk and Suzuki, 1980). First, the sense of polarisation is the same for both the fundamental and harmonic components in each of the

fundamental-harmonic pairs observed. The fundamental component is known to be polarised in the sense of the o -mode. Second, related type I and type U bursts (from the same source) have the same sense of polarisation as harmonic type III bursts, both of which are known to favour o -mode emission. For $\Omega_e/\omega_p \gtrsim 1$, the x -mode emission rate is significantly higher than the o -mode emission rate, with $r \approx -1$. Such high degrees of polarisation are not observed in type III bursts. This implies that $\Omega_e/\omega_p \lesssim 1$ is always satisfied in type III sources, provided that depolarisation effects are not too significant. Depolarisation effects due to the propagation of radiation through the coronal plasma can lead to lower observed r than that produced at the source of emission. For example, observed r from the solar limb are generally lower than from the centre (Dulk and Suzuki, 1980) because this radiation passes through more coronal plasma to reach an observer. By substituting $\Omega_e/\omega_p \lesssim 1$ into (42), with $\chi \approx \pi/4$ at the peak of emission, we obtain $r \lesssim 0.16$. This condition is satisfied for the majority of harmonic bursts shown in Figure 1. However, as for the earlier theory (assuming the head-on and weak-field approximations), the small fraction of observed bursts with higher degrees of polarisation ($r > 0.16$) cannot be explained in this regime.

(ii) For faster beam speeds, with $k_{\text{beam}} \gtrsim k_T$, the head-on approximation is completely invalid. In this regime, the preferred sense of polarisation at the peak of emission can be either x -mode (negative r) or o -mode (positive r), depending on the magnitude of the wave-number offset between the beam-driven and backscattered Langmuir (z -mode) waves. Significantly higher values for r (in either sense) can be produced than predicted by (1), where the head-on and weak-field approximations are assumed. This regime is necessary to account for observed $r \gtrsim 0.16$, which apply both to a small fraction of the fundamental-harmonic pairs (see Figure 1) and to a fraction of structureless type III bursts (Mercier, 1990). Although high degrees of polarisation can be produced in favour of either mode (assuming an offset in the backscattered Langmuir waves), it is likely that the majority of observed emission with high r is produced in favour of the o -mode, because higher wave levels are generally produced in this mode. For example, in Figures 14 and 15, x -mode emission peaks at $\chi \approx 10^\circ$, with $r \approx -0.4$, and o -mode emission peaks at $\chi \approx 26^\circ$, with $r \approx 0.45$. In this case, the peak in o -mode emission is at nearly twice the rate of x -mode emission. For such high degrees of polarisation, lower coronal magnetic fields are predicted than if (1) is assumed. It is also possible that lower values of r ($\lesssim 0.16$) are produced in this regime, for intermediate offsets between $k_0 = 0$ and k_T and/or for lower Ω_e/ω_p . The harmonic emission in fundamental-harmonic pairs (Dulk and Suzuki, 1980) is known to be polarised in favour of o -mode emission. An offset in the backscattered Langmuir waves is therefore necessary, in this regime, to produce this bias. It is not clear whether structureless type III bursts (Mercier, 1990) are polarised in favour of the o -mode or the x -mode, although, at least for the high observed values of r , it is more probable that o -mode emission is favoured, because of the faster o -mode emission rate.

Thus by relaxing the assumption of the head-on approximation, we can account for high observed r in harmonic type III bursts. This was not possible in the earlier theory, where the head-on and weak-field approximations were assumed. Note that high values of r are uncommon for harmonic type III sources, and hence the conditions required for high degrees of polarisation to be produced are presumably not normally satisfied. The required conditions are fast beams, high values of Ω_e/ω_p and a significant wave number offset in the backscattered Langmuir waves. One testable prediction (for verification of this theory) is that observed harmonic type III bursts with high degrees of polarisation should correlate with the fastest electron beams associated with harmonic emission.

Overall we conclude that in both regimes, an estimate for the coronal magnetic field may only be made if the form of the Langmuir wave-number spectra, and in particular the magnitude of the offset between the beam-driven and backscattered Langmuir waves, is known. This requires knowledge of the beam and plasma properties at the source of harmonic type III emission.

In the final paragraphs of this discussion we consider the possible reinterpretation of earlier type III polarisation measurements, and the application of the revised theory to relativistic type IIIId bursts and the reversal of polarisation sense in type V bursts. Benz and Zlobec (1978) observed a positive correlation between degree of polarisation and drift rate in type III bursts. Central to their analysis was the assumption that there exist two distinct populations in their data. The first population of relatively high polarisation bursts, for which a correlation between degree of polarisation and drift rate is evident, were assumed to be fundamental bursts, and the second population of bursts with low polarisation and no correlation with drift rate were assumed to be harmonic. This was in correspondence with the existing theory. In the light of the revised theory, it is possible that a number of the high polarisation bursts are in fact harmonic, although clear identification between fundamental and harmonic bursts is required to test the predictions of this theory. However, if this is the case, then the observed correlation between degree of polarisation and drift rate is in accordance with our predictions.

Strong observational evidence exists that fast-drift type IIIId bursts are harmonic radiation (Poquérousse, 1994). The degree of polarisation has not yet been measured for these bursts. The validity of this theory in treating this class of bursts depends on whether the electrostatic backscatter decay process occurs (to produce backward propagating Langmuir waves). The condition $k_{\text{beam}} \geq k_0/2$ must be satisfied in order for the backscatter decay process to proceed (Cairns, 1987), with k_0 given by (41). For typical type IIIId burst parameters, $k_{\text{beam}} \approx k_0/2$, so it is likely that backscatter decay is suppressed. In this regime, it is more likely that the second harmonic is produced directly by coalescence of two Langmuir waves propagating in roughly the same direction, with $k_{\text{beam}} \lesssim k_T$ (Willes, Robinson, and Melrose, 1996). The theory for the polarisation of second harmonic emission in this regime has not yet been formulated. However, in instances where this theory is valid (with

$k_{\text{beam}} \geq k_0/2$), we predict that high degrees of polarisation should be produced for the fast drift bursts.

Finally, we comment on the polarisation reversal in type V bursts, from o -mode in the preceding type III burst to x -mode in the type V radiation (Dulk, Suzuki, and Gary, 1980). The favoured explanation (Dulk, Suzuki, and Gary, 1980) relies on a reversal in the preferred sense of polarisation (from o -mode to x -mode) with increased isotropy of the Langmuir waves (from alignment with the magnetic field direction to isotropic). Preliminary results show that increased isotropy of the Langmuir waves implies lower r (i.e., increased x -mode polarisation), in agreement with previous theory. Work is still in progress on this problem.

6. Conclusion

In this paper, we have considered the simultaneous wave emission processes $Z' + Z'' \rightarrow X, O$, where two z -mode (magnetised Langmuir) waves coalesce to produce either an x -mode or an o -mode wave at twice the plasma frequency. The relative x - and o -mode emission rates are related to the degree of polarisation r , which is an observable quantity. The theory for the polarisation of harmonic type III bursts has been improved in two ways. Firstly, two simplifying approximations have been relaxed; namely the head-on approximation, which is only valid for beam-induced Langmuir wave numbers $k_{\text{beam}} \gg k_T$ (where k_T is the product x -mode or o -mode wave number), and the weak-field limit, which assumes weak coronal magnetic fields. Secondly, we have assumed physically realistic Langmuir wave-number spectra which include the wave-number offset between beam-driven and (oppositely-directed) backscattered Langmuir waves.

The main conclusions are:

(i) The fraction of observed emission with high degrees of polarisation, which could not be explained in earlier theories (with the above-mentioned simplifying approximations), can be explained once the head-on and weak-field approximations have been relaxed. Values of $r > 0.16$ require $k_{\text{beam}} \gtrsim k_T$ (where the head-on approximation breaks down), reasonably high values of Ω_e/ω_p , and an offset in the backscattered Langmuir waves. Because such high values for r can only be produced by fast beams, a correlation should be observable between the drift rate of the bursts and the degree of harmonic polarisation. Although either x -mode or o -mode emission can dominate, depending on the magnitude of the wave-number offset in backscattered Langmuir waves, high degrees of polarisation $r > 0.16$ are most likely to favour o -mode emission.

(ii) In situations where the head-on approximation is reasonably well satisfied, lower values of r are predicted (at the peak emission rate) than if the head-on and weak-field approximations are assumed. As in earlier theory, o -mode emission is typically favoured in this regime.

(iii) The predicted degree of polarisation is strongly dependent on the magnitude of the wave-number offset between beam-driven and backscattered Langmuir waves. Therefore, any attempts to estimate coronal magnetic field strengths from polarisation measurements requires knowledge of beam and plasma parameters in harmonic type III sources.

(iv) The condition $\Omega_e/\omega_p \lesssim 1$ is always satisfied in type III sources. Otherwise strong x -mode polarisation (with $r \approx -1$) would be observed.

Acknowledgements

The authors thank P. A. Robinson for useful discussions and comments on the manuscript and G. A. Dulk for suggesting further applications for the theory.

This work was supported by an Australian Postgraduate Award.

Appendix

In this Appendix we outline the method for the numerical evaluation of the emission rate $dI_T(\mathbf{k})/dt$ (34), given the frequency ω_T and angle of propagation χ of a transverse (x - or o -mode) wave. Figure 16 displays a flow chart of the sequence of steps necessary to numerically evaluate the integral (34). In the following paragraphs we expand on the material presented in the flowchart.

The first step is to calculate the transverse wave number k_T from the magnetoionic mode dispersion relation (34), as shown in the upper graph in Figure 16. The integral (34) is evaluated by numerical two-dimensional Simpson's integration over the angles θ' and ϕ' of the first coalescing z -mode wave. The region of integration is in fact much smaller than $0 \leq \theta' \leq \pi$ because of the limited angular extent of the z -mode wave-number spectrum (the Gaussian spectrum peaks at $\theta' = 0$ for the forward component, and $\theta' = \pi$ for the backward component). When considering high wave number z -mode waves (where the wave frequency is close to the z -mode resonance ω_{zr} (13)), the integrand of (34) peaks about θ_{\max} , where

$$2\omega_{zr}(\theta_{\max}) = \omega_T, \quad (43)$$

which yields the two values

$$\theta_{\max} = \cos^{-1} \left[\pm \left(\frac{\omega_T^2(\omega_p^2 + \Omega_e^2) - \omega_T^4/4}{4\omega_p^2\Omega_e^2} \right)^{1/2} \right]. \quad (44)$$

The values for k' , k'' , θ'' , and ϕ'' are now found by iteration. An initial value k'_+ is chosen for k' , well in excess of k_f (the peak wave number of the forward z -mode wave-number spectrum), and then calculating $g(k'_+)$ from (33). k' is then

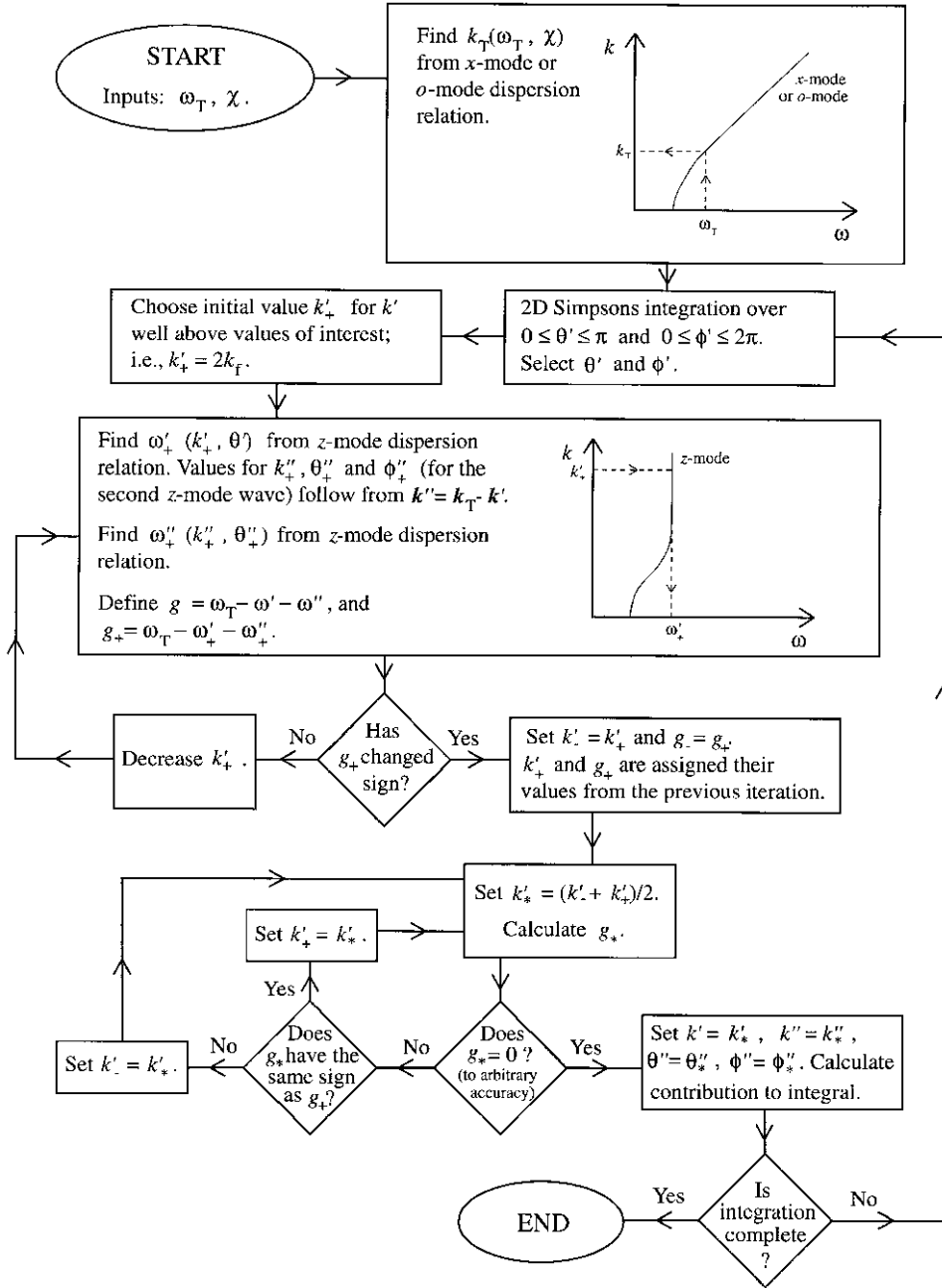


Figure 16. Flowchart illustrating the steps taken in the numerical evaluation of the emission rate (34).

decreased by increments until $g(k'_+)$ changes sign. The following steps are taken in calculating $g(k'_+)$:

(i) The z -mode wave frequency ω'_+ is calculated from the z -mode dispersion relation (8), knowing both k'_+ and θ' .

(ii) Values for k''_+ , θ''_+ , and ϕ''_+ follow from $\mathbf{k}'' = \mathbf{k}_T - \mathbf{k}'$, with

$$k''_+{}^2 = k'_+{}^2 + k_T^2 - 2k'_+k_T(\sin\theta'_+ \cos\phi'_+ \sin\chi + \cos\theta'_+ \cos\chi), \quad (45)$$

$$\theta''_+{}^2 = \cos^{-1} \left(\frac{k_T \cos\chi - k'_+ \cos\theta'_+}{k''_+} \right), \quad (46)$$

$$\phi''_+ = \sin^{-1} \left(\frac{-k'_+ \sin\theta'_+ \sin\phi'_+}{k''_+ \sin\theta''_+} \right), \quad (47)$$

$$\phi''_+ = \cos^{-1} \left(\frac{k_T \sin\chi - k'_+ \sin\theta'_+ \cos\phi'_+}{k''_+ \sin\theta''_+} \right). \quad (48)$$

Both (47) and (48) are required to determine which quadrant ϕ''_+ lies in.

(iii) The z -mode wave frequency ω''_+ is calculated from the z -mode dispersion relation (8), knowing both k''_+ and θ''_+ .

(iv) $g(k'_+)$ is calculated from (33).

Once $g(k'_+)$ has changed sign (after say, n iterations), we define $k''_-, k''_+, \theta''_-, \theta''_+$, and ϕ''_- to be the values of $k', k'', \theta',$ and ϕ'' at the n th iteration, and $k'_-, k'_+, \theta'_-, \theta'_+$ and ϕ''_+ by their values at the $(n-1)$ th iteration. A binary search between k''_- and k''_+ is then undertaken to find the value of k' at which $g(k') = 0$ (to desired accuracy).

References

- Benz, A. O. and Zlobec, P.: 1978, *Astron. Astrophys.* **63**, 137.
 Cairns, I. H.: 1987, *J. Plasma Phys.* **38**, 179.
 Dulk, G. A. and McLean, D. J.: 1978, *Solar Phys.* **57**, 279.
 Dulk, G. A. and Suzuki, S.: 1980, *Astron. Astrophys.* **88**, 203.
 Dulk, G. A., Suzuki, S., and Gary, D. E.: 1980, *Astron. Astrophys.* **88**, 218.
 Melrose, D. B.: 1986, *Instabilities in Space and Laboratory Plasmas*, Cambridge University Press, Cambridge.
 Melrose, D. B. and Sy, W. N.: 1972, *Australian J. Phys.* **25**, 387.
 Melrose, D. B., Dulk, G. A., and Gary, D. E.: 1980, *Proc. Astron. Soc. Australia* **4**, 50.
 Melrose, D. B., Dulk, G. A., and Smerd, S. F.: 1978, *Astron. Astrophys.* **66**, 315.
 Mercier, C.: 1990, *Solar Phys.* **130**, 119.
 Poqu russe, M.: 1994, *Astron. Astrophys.* **286**, 611.
 Robinson, P. A., Willes, A. J., and Cairns, I. H.: 1993, *Astrophys. J.* **408**, 720.
 Willes, A. J., Robinson, P. A., and Melrose, D. B.: 1996, *Phys. Plasmas* **3**, 149.
 Zlotnik, E. Ya.: 1981, *Astron. Astrophys.* **101**, 250.